energies

MDPI

Article

Steps towards Decarbonization of an Offshore Microgrid: Including Renewable, Enhancing Storage and Eliminating Need of Dump Load

Norma Anglani [1], Salvatore R. Di Salvo [1], Giovanna Oriti [2,*] and Alexander L. Julian [3]

[1] Electrical, Computer and Biomedical Engineering Department, University of Pavia, 97100 Pavia, Italy
[2] Department of Electrical and Computer Engineering, Naval Postgraduate School, Monterey, CA 93943, USA
[3] Independent Researcher, Seaside, CA 93955, USA
* Correspondence: goriti@nps.edu

Abstract: A novel control strategy to manage the integration of a wind turbine (WT) and an energy storage unit to an existing stand-alone microgrid servicing an oil and gas (O&G) rig is the topic of this paper. The control strategy includes a primary and a secondary controller that, using the battery in tandem with the WT, does not require any dump load (A). The secondary controller includes an energy management system (EMS) which uses the estimated wind production and other specific local information to size the battery to avoid the curtailment of the WT (B) and simultaneously provide the framework for the economic analysis (C). Points A, B and C are the main novelties introduced with this work. Additionally, a primary controller operates the original microgrid source, a gas turbine (GT), at its maximum efficiency through an active power control strategy to lower fuel consumption, by prioritizing the exploitation of the renewable energy source through the combination EMS and battery sizing. The microgrid is simulated and the combined controller of the battery and GT bench-tested.

Keywords: microgrids; oil and gas; energy management; primary control; gas turbine; renewable energy source integration; energy storage system; battery sizing; decarbonization

Citation: Anglani, N.; Di Salvo, S.R.; Oriti, G.; Julian, A.L. Steps towards Decarbonization of an Offshore Microgrid: Including Renewable, Enhancing Storage and Eliminating Need of Dump Load. *Energies* **2023**, *16*, 1411. https://doi.org/10.3390/en16031411

Academic Editors: Tek Tjing Lie and Noradin Ghadimi

Received: 10 November 2022
Revised: 16 December 2022
Accepted: 23 January 2023
Published: 31 January 2023

1. Introduction

The increased use of renewable and distributed energy sources in remote areas highly relies on the development of microgrids as a solution for their reliable integration. A microgrid control system is key to retrofitting existing stand-alone power systems where the only energy source burns fossil fuel, as is the case for an oil and gas (O&G) rig system and its services. Microgrids can operate both in grid-connected and stand-alone mode and their control systems must be designed to operate through challenging conditions such as low inertia and stability issues, which can be caused by renewable intermittent energy sources such as solar and wind generators. The bidirectional power flow must be managed by controlling the output voltages and currents of each source, thus securing the power balance and load-frequency control at the point of common coupling (PCC) [1].

1.1. Literature Review

Typically, microgrid control systems include three layers: primary, secondary an tertiary controllers. Primary controllers are the local controller of each distributed energy source/device, featuring the fastest response. Secondary controllers are the energy management systems, while tertiary controllers set the operating points for the microgrid according to the host requirements [2]. A comprehensive review of microgrid characteristics and controllers is available in [1,3–5].

Stand-alone or islanded microgrids are disconnected from the main grid and their control can be more challenging than the control of grid-connected microgrids due to the

lack of the reference parameters provided by the main grid. Islanded AC microgrids require a primary controller for the voltage source inverter that provides the microgrid voltage parameters, i.e., amplitude, frequency and phase angle. Robust control schemes for such grid-forming converters are presented in [2,6]. Isolated microgrids need a secondary controller to determine the optimal dispatch and schedule of the distributed energy resources to achieve reliable operations [7].

Around the world the use of stand-alone microgrids is the only solution to provide electricity to remote areas. According to [8] in Canada there are 280 off-grid communities across the nation and around the world such grid-tied and remote microgrid projects have overcome 8000 in the third quarter of 2022 [9].

Stand-alone microgrids are also required on islands and especially in offshore locations. Fard and Tedeschi in [10] present a review of the conventional offshore loads, such as O&G platforms, sub-sea processing plants, deep-sea mining and aquaculture applications.

On O&G platforms electricity is usually provided by diesel generators or gas turbines (GT), leading to significant greenhouse gas emissions. To reduce the environmental impact, renewable energy resources are being added to O&G rig microgrids. Previous literature such as [11–13] present feasible examples of integration and predict fuel savings and the reduction of greenhouse gasses. In [11], critical scenarios are investigated in AC microgrids with respect to stability. In [12,13] an energy management method for a microgrid including two (GT) in parallel with a wind turbine (WT) was proposed, while [14,15] propose a decentralized control strategy for offshore microgrids dominated by large WT working in tandem with conventional diesel generators. Although these papers demonstrate how to operate the microgrids, they don't include any economic consideration or the rational for the energy management system.

More recent studies [16,17] focused on the microgrid energy management with the goal to compensate for the variability of the output power produced by WTs in the short-term. The authors proposed the use of a dump load to reduce the effect that abrupt changes in wind power production have on grid stability. This work was later expanded in [18] with the addition of an energy storage system.

1.2. Novel Contribution and Paper Organization

In recent years many papers have addressed microgrid technology and microgrid control methods, however the previous section identifies a gap in literature which is retrofitting stand-alone microgrids in O&G rigs with the specific goal of reducing fuel consumption over the lifetime of the rig.

The scope of this work, where we show how the validity of the procedure in [19] can be extended and validated on the components with a bench-test on a 3 phase configuration, is to analyze how to retrofit an existing service for an offshore oil rig (an injection pump to fluidify the crude oil in the pipelines, resting on the seabed, which, due to the deepness of the sea, may experience very low temperature), while introducing renewable energy sources. Our focus is on the role that energy storage can play in eliminating the operation of a dump load to make better use of the renewable energy that is available, thus accelerating the energy transition towards the decarbonization of such a service. The methodological economic approach is introduced by highlighting the major components and their dependencies to support the choices deriving from the methodological approach. Furthermore, this paper presents primary and secondary controllers for a power electronics system which integrate renewable energy sources and storage into a fossil fuel fed microgrid. We propose an energy storage sizing method to "virtually" eliminate the curtailment of the newly integrated renewable sources without using dump loads, and we provide the economic grounds to support the choice of the transition towards a more sustainable service.

The proposed control system addresses all the aspects discussed in previous literature:

- it manages the microgrid power sources using a novel energy management system (EMS), focused on our main objectives, as reported in Section 3;

- does not require a dump load, because the battery bank is sized to eliminate its need, as reported in Section 3.1;
- includes a primary controller designed to manage the output power of the generator, to maximize its efficiency and keep the GT running as little as possible, as demonstrated in Section 4.

The paper is structured as follows: Section 2 presents the model of the proposed microgrid at the service of an offshore platform and the primary control system to minimize fuel consumption. Section 3 presents the combination between the energy management algorithm and the battery sizing method, thus ensuring the scope of exploiting the renewable at its best, and -as a consequence- decreasing the fuel consumption as much as possible. In Section 4 the simulation results are discussed and Section 5 presents the experimental validation of the primary controller on a laboratory prototype. Section 6 discusses the economic methodology to support the validity of the energy storage sizing. Finally, Section 7 presents the conclusions.

2. Primary Controller

This work proposes a primary controller for a battery energy storage system (BES), employed on an isolated O&G microgrid mainly supplied by the GT and a location-specific renewable energy resource, which in this paper is a WT (see Figure 1).

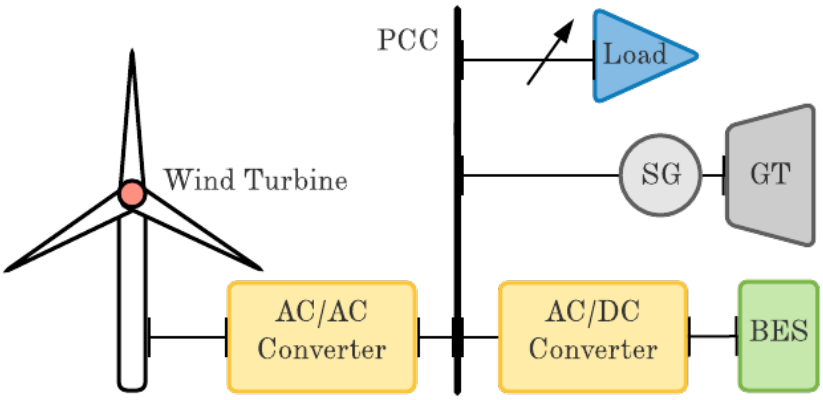

Figure 1. Representation of the microgrid model for the case study. The arrow indicates a variable load.

The aim is to have the grid working with as little fuel as possible by ensuring (i) the operation of the GT at its maximum efficiency when it is on, (ii) the maximum renewable deployment and (iii) by ensuring that no dump loads are used to curtail the renewable production.

The primary controller is developed for a dual stage BES power conversion system, comprising a bidirectional boost converter connected through a DC-link to a two-level, three-phase inverter. An LC filter is used to connect the inverter to the microgrid AC bus, as in Figure 2. Two different control loops are used, the bidirectional boost regulates the battery current (I_{bat}) and the dc-link voltage (V_{DC}), while the inverter controls the power exchanged with the AC microgrid.

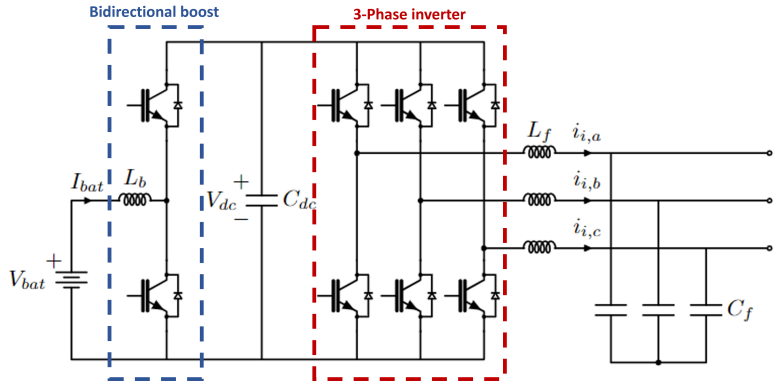

Figure 2. Converter dual stage topology with bidirectional boost converter and two-level three-phase inverter with LC filter.

2.1. Bidirectional DC-DC Converter Control

Two cascaded control loops are used for the control of the bidirectional boost converter; the inner loop regulates the battery current I_{bat}, and the outer loop controls the dc link voltage V_{dc}, as shown in Figure 3. PI controllers are chosen for both control loops, thus the transfer functions $G_v(s)$ and $G_c(s)$ can be written as

$$G_v(s) = K_{p,v} + \frac{K_{i,v}}{s} \tag{1}$$

$$G_c(s) = K_{p,c} + \frac{K_{i,c}}{s} \tag{2}$$

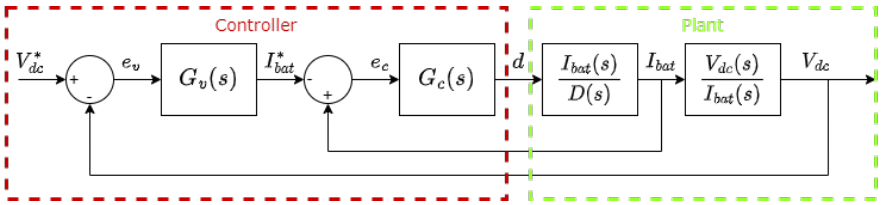

Figure 3. Block diagram of the bidirectional boost converter control.

In order to find the transfer functions of the battery current over the duty cycle $\frac{I_{bat}(s)}{D(s)}$ and the dc-link voltage over the battery current $\frac{V_{dc}(s)}{I_{bat}(s)}$ small-signal analysis of the boost circuit with an equivalent resistor representing the inverter is performed [20]. The bidirectional boost converter can have two different equivalent circuits depending on the switching states as shown in Figure 4. When the top switch is conducing, Figure 4a, the battery current and dc-link voltage equations can be written as

$$L_b \frac{d\, i_{bat}}{dt} = V_{bat} - V_{dc} \tag{3}$$

$$C_{dc} \frac{d\, v_{dc}}{dt} = i_{bat} - \frac{V_{dc}}{R_{eq}}. \tag{4}$$

When the bottom switch is on, Figure 4b, the converter's equations are

$$L_b \frac{d\, i_{bat}}{dt} = V_{bat} \tag{5}$$

$$C_{dc} \frac{d\, v_{dc}}{dt} = -\frac{V_{dc}}{R_{eq}} \tag{6}$$

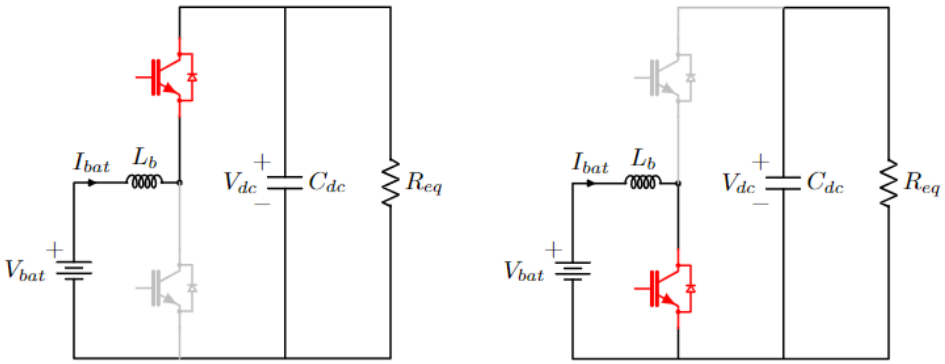

(**a**) Top switch ON (**b**) Bottom switch ON

Figure 4. Bidirectional boost converter states.

By averaging the dc-link voltage and the battery current over the switching period T_s and applying the small signal perturbation to Equations (3)–(6), the following equations are obtained

$$L_b \frac{d\,\hat{i}_{bat}}{dt} = -\bar{V}_{dc}\hat{d} - \bar{D}\hat{v}_{dc} \tag{7}$$

$$C_{dc}\frac{d\,\hat{v}_{dc}}{dt} = \bar{I}_{bat}\hat{d} + \bar{D}\hat{i}_{bat} - \frac{2}{R_{eq}}(\bar{V}_{dc}\hat{d} + \bar{D}\hat{v}_{dc}). \tag{8}$$

where d is the duty cycle, and the capital letters with "¯" symbol represent the steady state value and small letters with "ˆ" symbol represent the small signal perturbation. Finally by applying the Laplace transform to Equations (7) and (8) i_{bat} and v_{dc} can be written as

$$\hat{I}_{bat}(s) = -\frac{\bar{V}_{dc}}{s\,L_b}\hat{D}(s) - \frac{\bar{D}}{s\,L_b}\hat{V}_{dc}(s) \tag{9}$$

$$\hat{V}_{dc}(s) = \frac{\bar{I}_{bat} - \frac{2}{R_{eq}}\bar{V}_{dc}}{s\,C_{dc} + \frac{2\bar{D}-1}{R_{eq}}}\hat{D}(s) + \frac{\bar{D}}{s\,C_{dc} + \frac{2\bar{D}-1}{R_{eq}}}\hat{I}_{bat}(s). \tag{10}$$

With the transfer function obtained in Equations (9) and (10) the two proportional-integral (PI) controllers are tuned so that the dynamics of the outer loop is ten times slower than the inner one, in order to achieve a stable operation of the converter.

2.2. Three-Phase Inverter Control

The block scheme of the primary controller of the three-phase inverter is shown in Figure 5. The aim is to control the output current of the inverter in order to keep the power output of the GT constant in order to maximize its efficiency. The control system includes two PI controllers in the $dq0$ synchronous reference frame. The angle of the phase-a of the output capacitor voltage is captured by a phase locked loop (PLL). This angle is necessary for the abc to $dq0$ and the $dq0$ to abc reference frame transformations [21].

The active power reference P_b^* is calculated as the balance between the target power of the GT (P_{gt}^*), the load power demand and the power output of the WT as

$$P_b^* = P_L - P_{gt}^* - P_{wt}. \tag{11}$$

The reactive power reference, Q_b^*, is kept to zero in order to achieve unity power factor.

From the power references P_b^* and Q_b^* the references dq currents are calculated and used in the current control loop. The controller output is transformed from $dq0$ to abc and sent to the PWM modulator. The gate signals are applied to the inverter switches.

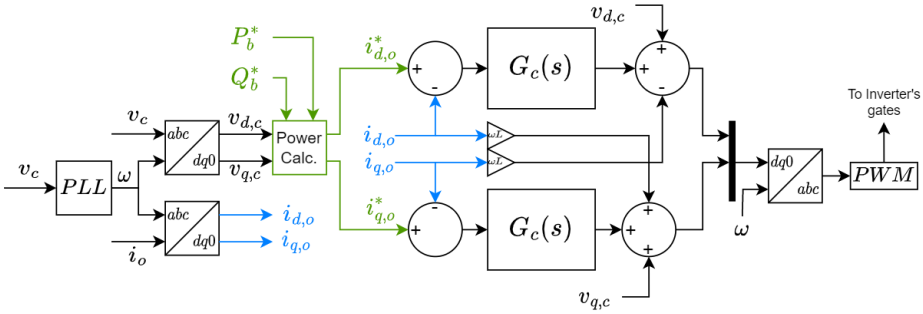

Figure 5. Block diagram of the primary control system.

3. The Energy Management System and the Role of the Battery Sizing

The proposed EMS, which is the secondary controller, was first introduced in [19], for a single-phase microgrid, and is depicted in Figure 6. It aims to (i) ensure the maximum renewable deployment, (ii) let the GT work at maximum efficiency and (iii) minimize load dumping, typical of higher power configurations. The flowchart in Figure 7. describes the most challenging mode of operation, when the WT surplus has to be managed without either curtailing or using a dump load. If the sizing of the battery is performed according to the procedure we envisage below, and appropriate data to represent the system has been correctly estimated/used, then neither the curtailment nor dump load are needed. On the contrary if an unexpected WT overproduction with respect to the load can not be managed, then priority #1 and #2 shall be foreseen to have the system operated, no matter what.

Power balance in the EMS (12) must be satisfied at every time t, at the point of common coupling.

$$\begin{aligned} &P_{gt}(t) + P_{wt}(t) = P_{load}(t) + P_b(t) \qquad \forall t \\ &P_b(t) = \begin{cases} P_b(t) \geq 0 & charge \\ P_b(t) < 0 & discharge \end{cases} \end{aligned} \tag{12}$$

where P_{gt} is the GT output power, P_{wt} is the WT output power, P_{load} is the power required by the load and P_b is the battery power. This variable is positive when the battery is charging and negative when the battery is discharging. The EMS algorithm accounts for the rating of the battery as well as the GT rated power and it shuts down the GT when it gets too close to the chocking area. Further, the EMS keeps the battery state of charge (SOC) between a minimum value SOC_{min} and a maximum value SOC_{max} and ensures that the battery power in both charging or discharging mode of operation remains within its specifications. The battery has been sized according to the best and worst daily energy production of the DER/RES, which in this case is a WT, (E_{wt}^b, E_{wt}^w) the maximum and minimum daily energy demand from the load (E_L^x, E_L^m) and the operating limits of the GT [19].

In Section 3.1 we report the logic for sizing the battery according to the meteorological conditions and the GT rating to avoid WT curtailment and to avoid sending power to a dump load. Additionally, "the GT must operate above its minimum power output to avoid mechanical wear and loss of efficiency and this can happen by relating it to the battery capacity" [19].

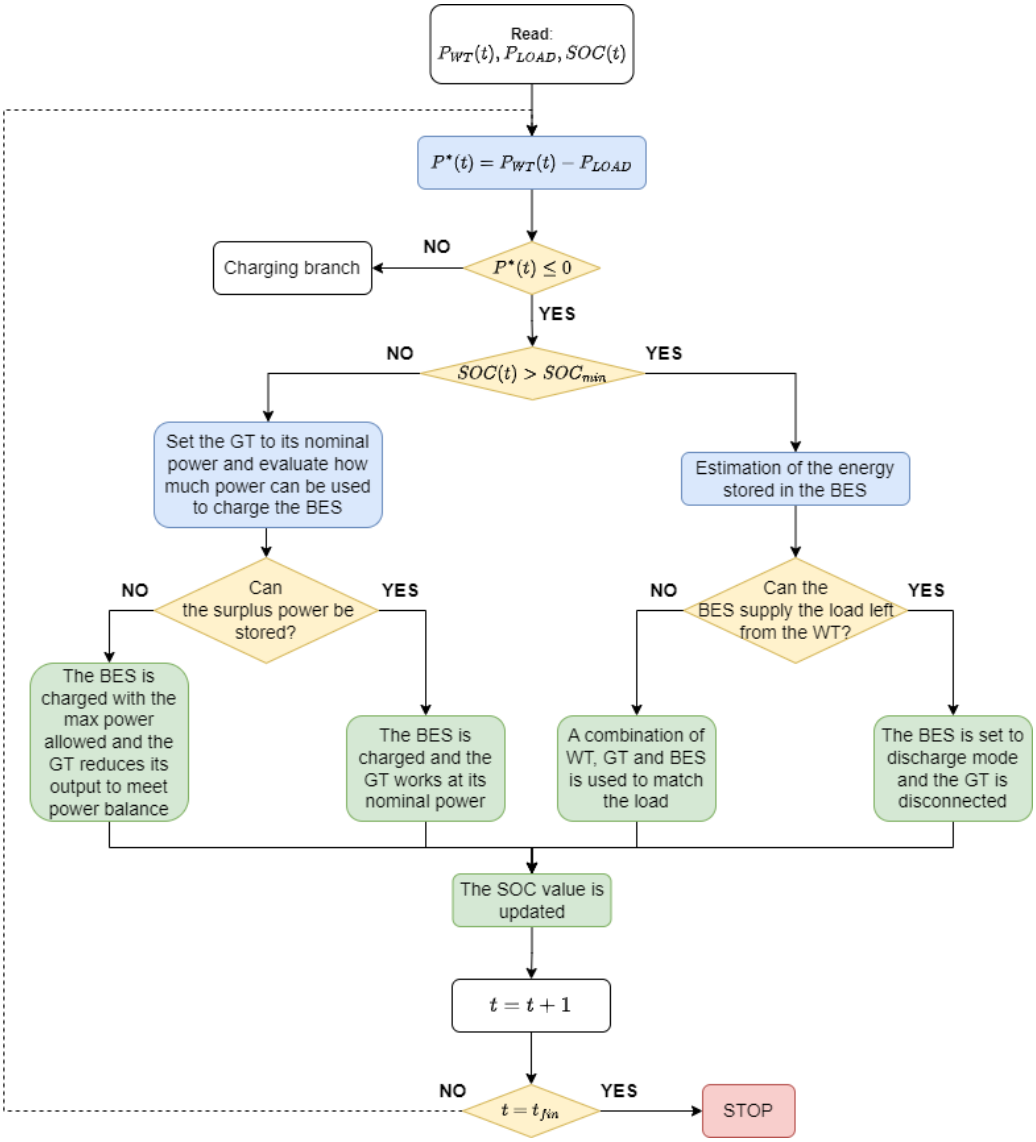

Figure 6. Novel EMS flowchart.

The economics in support of this choice and its implications are discussed in Section 6 and take into account all the major parameters affecting the microgrid cost-effectiveness, such as the time horizon over which a O&G rig is going to be operative, the capital cost of the extra capacity for the battery, the economic value of the avoided curtailment and the savings due to a missing (or highly reduced) dump load.

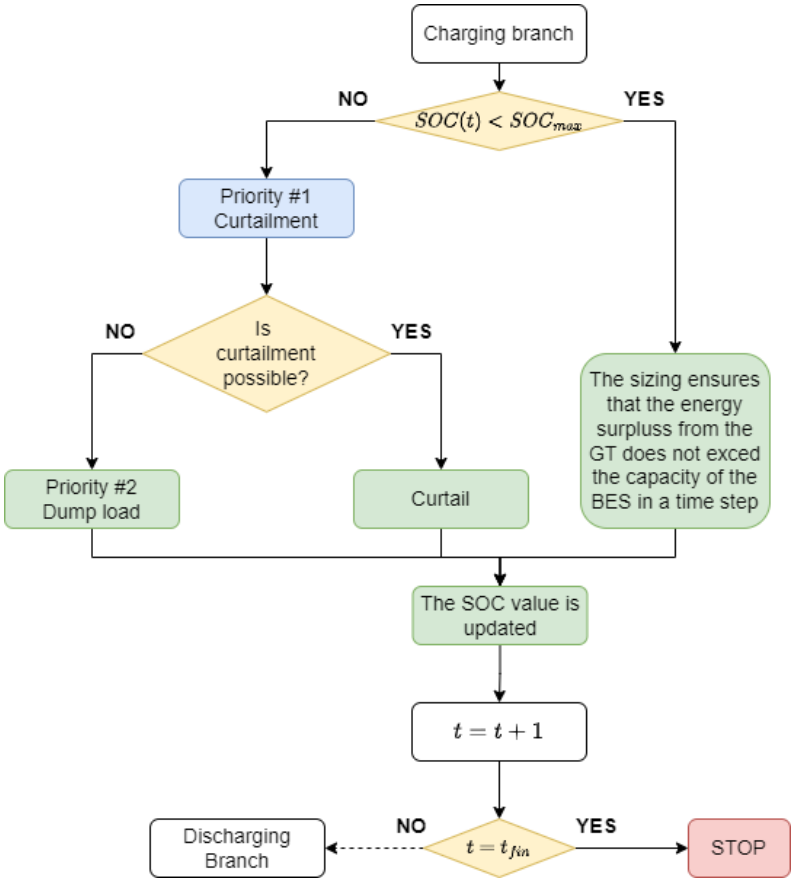

Figure 7. Rule-based flowchart of the proposed EMS left branch of Figure 6. Focus on the role that the management of WT-battery-GT plays in case of surplus from WT.

3.1. A New Sizing Methodology for the Battery, Supplementary to the EMS

The battery size is determined after the rating of the load, WT and the GT are known and using meteorological data. Note that the GT is the existing turbine originally sized to service the full load. In the presence of retrofitting, where the GT was already there and the WT was already sized for the maximum production, a novel way for sizing the battery is proposed, to potentially use neither curtailment nor dump loads.

The daily energy production, with E^b_{wt} being the best and E^w_{wt} being the worst, is identified by assessing the best and the worst day using the WT data-sheet and by analyzing the wind data records (usually 10 years) available for the specific site in which the oil rig is located. There are several methods and also software to help optimize the mix of sources (Homer, RETscreen) but as explained above, this is not the focus of the work presented in this paper, so we will neglect considerations on how to get such data. Nevertheless a few comments, about the role that using deterministic data for our EMS, are due. While using real instead of forecasted data is not an issue for a rule-base procedure as that of Figures 6 and 7, the difference between the expected and the real data may be an issue for the sizing of the battery. Usually, load and local weather conditions are not deterministic data when talking about power, but the intrinsic nature of this load (a pump for an intermittent and predetermined operation) made us consider it as deterministic, without compromising the validity of the procedure. A different reasoning is applied for the WT production data and assumptions. For instance, in [22] and (more in details) in [23], the methodology for using 10 years of data for a feasibility study is reported and discussed for projecting production data of a wave energy converter. It overcomes the stochastic approach, by referring to the *best* and *worst day*, referring to the renewable energy production, here adopted for the WT. Note that the scope of this paragraph is not to propose a specific methodology to assess the worst and the best daily production, but to guide in the

procedure which does use them. How to size the WT is alone a line of research, and it is out of the scope of this paper to comment on the methodology to get the required data for the proposal following below. Indeed, our focus is to provide a methodological framework to support the transition towards a *better fitted system*, which anyway is not at all supposed to be an *optimized system*: this retrofit takes care of the storage in combination with the tailored EMS in the light of a step by step procedure to decarbonize an offshore service. For the purpose of this scientific work we only assume that, whatever the sizing choice for the WT was, we make the most of that very choice only by using the data following from that decision.

The same daily calculation is performed on the load (maximum and minimum E_L^x, E_L^m, respectively) and on the GT (E_{gt}^x and E_{gt}^m), whose units are all kWh/day. The minimum value of GT electricity production can be derived similar to the evaluation done in [24], by using the reference to the minimum load factor x_{min}. Once the above energies are assessed (in kWh/day) then we set the following parameters and verify the following relationships as in [19], depending on E_{gt}^x (=P_{gt}^{rated}x24):

$$Load \quad \alpha = \frac{E_L^x}{E_{gt}^x} \tag{13}$$

$$\beta = \frac{E_L^m}{E_{gt}^x} \tag{14}$$

$$WT \quad \gamma = \frac{E_{wt}^w}{E_{gt}^x} \tag{15}$$

$$\delta = \frac{E_{wt}^b}{E_{gt}^x} \tag{16}$$

$$GT \quad x_{min} = \frac{E_{gt}^m}{E_{gt}^x} \tag{17}$$

where α, β, γ and δ have values smaller than 1 (meaning that E_{gt}^x is the greatest value among all, under the following assumptions). All the above ratios represent the fraction of the considered item with respect to the maximum daily GT production of the pre-retrofitting *only* supply. For instance α represents the ratio between the maximum daily load and the 24-h available supply from the GT, instead β is the ratio when the minimum daily load is considered. When the load is a repetitive service $\alpha \approx \beta$.

In order to maximize the efficiency of the GT so that it runs above the minimum allowed load factor x, the battery capacity has to be the buffer for all the extreme cases that may occur, that is:

$$E_b^c = E_{gt}^x + E_{wt}^b - E_L^m = E_{gt}^x.(1 + \delta - \beta) \quad charging\ mode \tag{18}$$

$$E_b^d = E_L^x - E_{gt}^m - E_{wt}^w = E_{gt}^x.(\alpha - \gamma - x_{min}) \quad discharging\ mode \tag{19}$$

and the variable ASE (battery necessary capacity) should be

$$ASE = E_{gt}^x.max\{(1 + \delta - \beta); (\alpha - x_{min} - \gamma)\} \tag{20}$$

Particularly, when

$$\gamma \leq x_{min} \leq \beta \leq \alpha \leq \delta \tag{21}$$

which means that when the maximum available daily wind production is greater than the maximum daily load and the minimum load its greater than the minimum available GT production. Then

$$\alpha - x_{min} - \gamma < 1 + \delta - \beta \quad \forall \alpha, \beta, \gamma, \delta, x_{min} \tag{22}$$

Following that, ASE is always equal to E_{gt}^{x}. $(1 + \delta - \beta)$ and in order to keep it as low as possible, then δ and β have to be similar in value so that ASE is $\approx E_{gt}^{x}$ (kWh/day). The condition that δ and β are similar in value means that in order to pursue our goal, which is to harness the RES production at the maximum without any need to use dump load, the best daily WT production shall be equal to the minimum daily load. When this load is a repetitive service, as the one considered, this assumption just means that the best WT production shall be similar to the load. And this is a reasonable and expected outcome.

The rated capacity Q can thus be:

$$Q = ASE/(1 - SoC_{min}) \tag{23}$$

No doubt that such sizing provides a noteworthy value, but in the overall it is likely that only a share of it can be considered the real addition (referred as *extra capacity* in Section 6). This is due to the fact that the microgrid configuration, where the RES integration is planned, already includes energy storage for safety reasons.

In this paper the battery capacity is determined with respect to the most relevant conditions, which ensure smaller depth of discharge (DoD) of the battery, and consequently a longer lifetime.

4. Simulation Results

The performance of the proposed controller was tested in a Matlab/Simulink model, Figure 8. The physics-based microgrid model includes a GT, a BES interfaced to the microgrid with the topology presented in the previous section and two resistive loads of 58 Ω and 14.5 Ω, one is kept constant and the other is activated through a breaker at half of the simulation. For the sake of simplicity the GT has been modelled as an ideal three pahse AC voltage source. The simulation parameters are reported in Table 1.

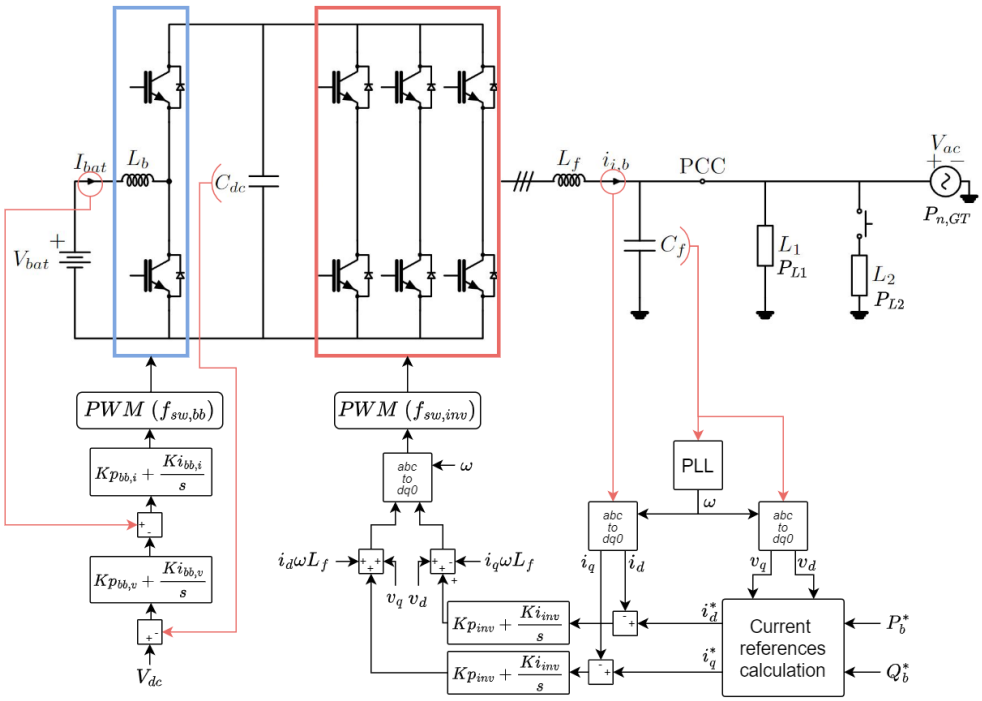

Figure 8. Block scheme of the model used for the simulation of the microgrid.

Table 1. Simulations parameters.

Converter Parameters					**Grid Parameters**				
L_f	0.6 mH	C_{dc}	3 mF	$P_{n,GT}$	300 W	V_{ac}	110 V	P_{L1}	105 W
C_f	30 µF	L_b	0.3 mH	V_{bat}	92 V	V_{dc}	160 V	P_{L2}	420 W
Controller Parameters						**Frequencies**			
$Kp_{bb,i}$	0.003	$Ki_{bb,i}$	2.4	f_0	60 Hz	$f_{sw,bb}$	12 kHz	$f_{sw,inv}$	10 kHz
$Kp_{bb,v}$	0.473	$Ki_{bb,v}$	18.68	T_{sim}	1 s	f_{clk}	2 MHz		
Kp_{inv}	2.188	Ki_{inv}	522.2						

Figure 9 shows the active power output during a 1 s simulation. In the first 0.33 s only load 1 is connected and it absorbs 105 W. During this part of the simulation the BES power is −200 W (charging) and the GT works at the determined set point. At 0.33 s the load 2 is connected and the battery power changes from −200 W to 200 W demonstrating that in response to a load step, the battery changes its output power according to the rules dictated by the energy management system in order to maintain the output of the GT at its nominal value

The GT picks up the transient due to the step change in the power demand. The primary controller reacts in 0.05 s and changes its power output in order to maintain the GT to 300 W. Finally, at 0.66 s the load 2 is disconnected and the BES is again set to −200 W. Also in this case the transient due to the step down in the load power demand lasts for 0.05 s and the GT output is kept to 300 W.

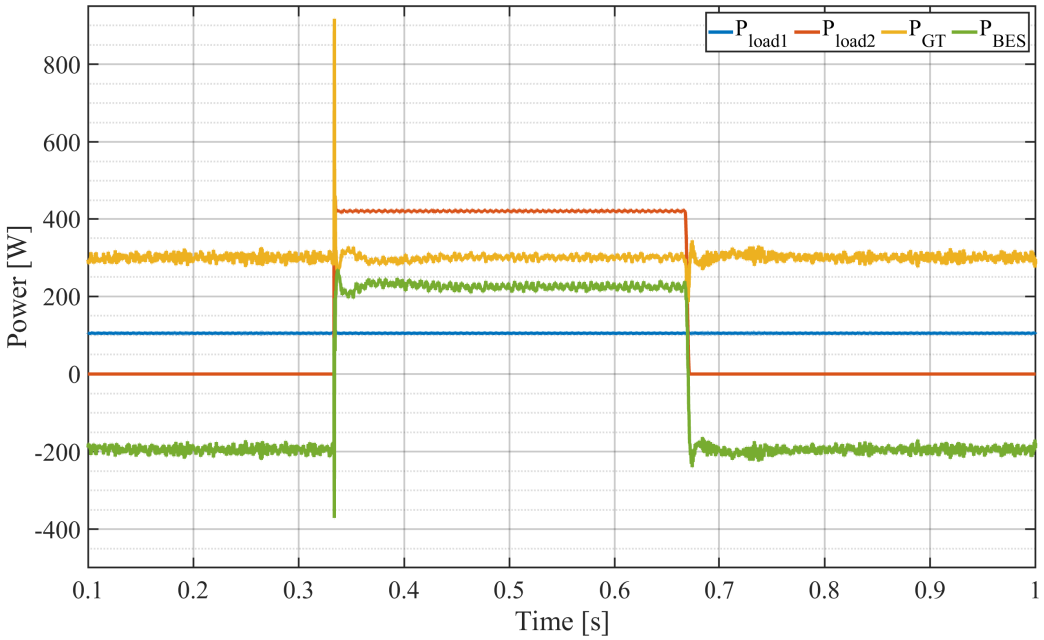

Figure 9. Active power measurement during one second simulation. P_{BES} is generic for P_b.

Figure 10 shows the reactive power output. In this case the reactive power from the BES is controlled to 0 *VARs* as expected. The reactive power absorbed from the grid is 0 *VARs* since two resistive loads are used in the simulations.

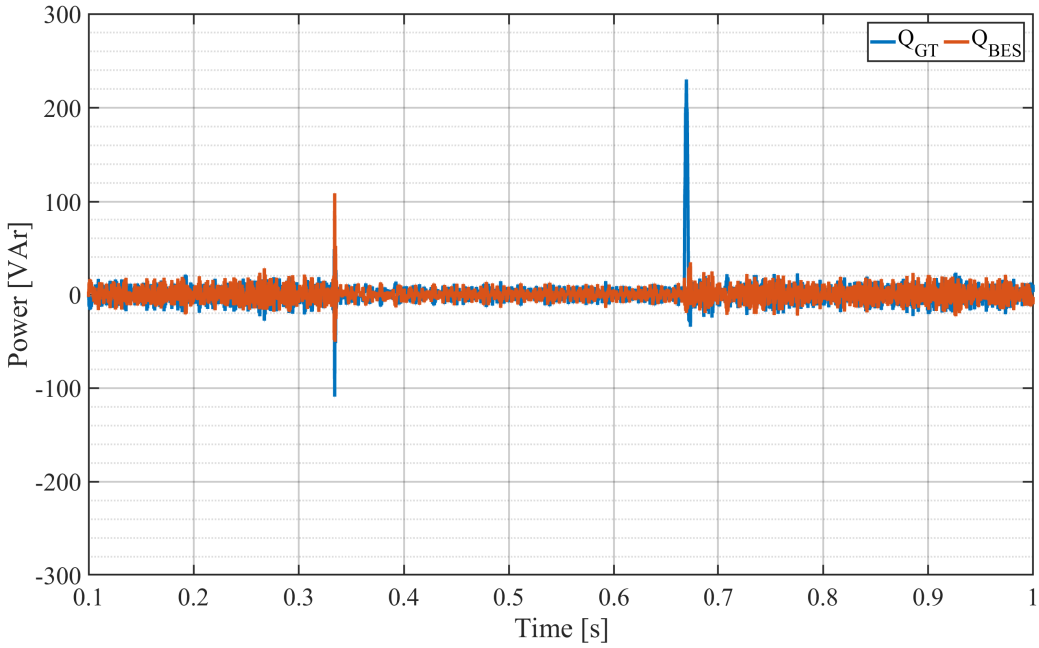

Figure 10. Reactive power measurement during one second simulation.

Figure 11 presents the DC-link voltage plot. The voltage is controlled as expected to its reference value of 160 V, the initial transient to regulate the capacitor voltage lasts for 0.1 s. When the step up and step down in the load power demand occur, respectively at 0.33 s and 0.66 s, the dc-link voltage presents some undershoots and overshoots of 5 V that are quickly compensated in 0.05 s. Such a transient is not an issue for the load serviced by this microgrid, which is a pump periodically injecting a thinner/fluid agent in the crude oil conduct. This service does not need a fast response because it is a repetitive action and delays that are fractions of a second do not affect the quality of the service itself, which is the ultimate goal of all the work presented in this paper.

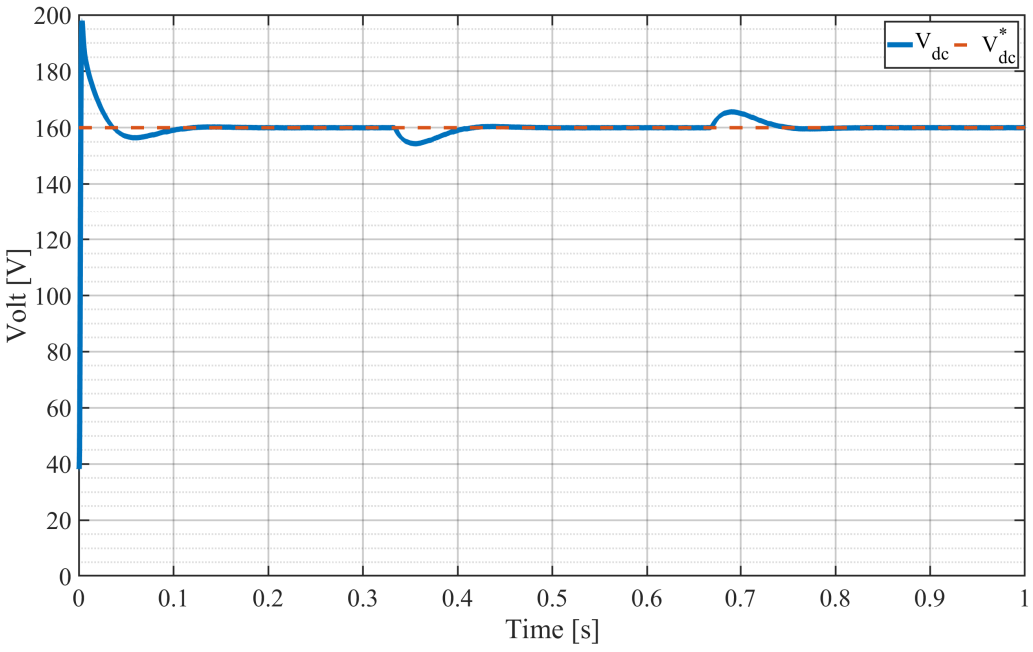

Figure 11. DC-link voltage measurement during one second simulation.

5. Experimental Validation

A laboratory prototype was built to validate the performance of the primary controller described in Section 2. The setup is shown in Figure 12, including a three-phase inverter with an LC filter and resistive loads. The inverter battery bus consists of eight, series-connected Genesis lead-acid batteries rated 12 V, connected in series and feeding a bidirectional boost converter. The 96 V battery voltage is boosted to 160 VDC. The GT is simulated using the laboratory utility power and a Variac. For validation of the primary controller shown in Figure 5 the line-to-line AC voltage was 78 Vrms (VGTa-VGTb).

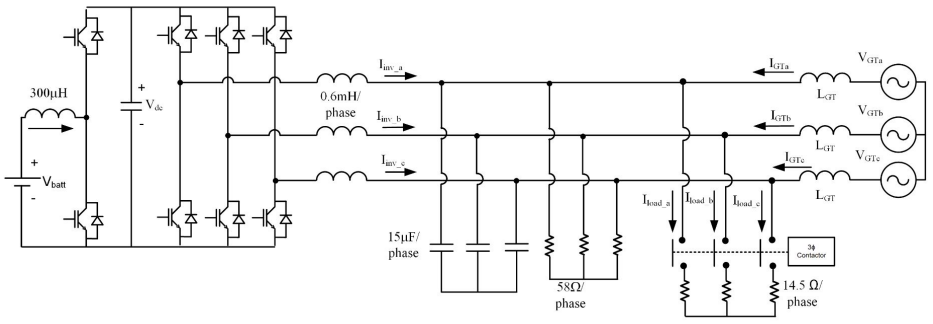

Figure 12. Circuit schematic of the laboratory layout for the experimental validation of the primary controller.

The control system was implemented on an OPAL-RT OP4510 real time control prototyping system, programmable via Matlab/SIMULINK software including OPAL-RT software. The GT reference power is set to 300 W so the source, which emulates the GT, delivers 300 W to the system at all times. When the three-phase contactor is open, power flows back to the batteries through the bidirectional boost to charge them because the load is less than 300 W ($P_{load} = 78^2/58 = 105$ W). If the batteries were fully charged then the reference power would be reduced. When the contactor is closed the inverter delivers power to the load since the load exceeds 300 W ($P_{load} = 78^2/58 + 78^2/14.5 = 524$ W).

Figure 13 shows the source power flow and the inverter power flow when the additional 14.5 Ω load is disconnected at t = 0 s. There is a delay in the transition because the mechanical contactor takes about 20 ms to activate, however the plots demonstrate the ability of the primary controller to compensate for the step in load, so that the source power returns to the set value within 0.4 s.

Figure 14 shows the load step up event demonstrating that the primary controller responds to the increase in load by supplying power from the batteries. The source power returns to its original value in about 0.4 s. Figure 15 shows the grid voltage (v_a) and inverter current (i_a) as the load turns on. The power flow reversal is noticeable where the current is initially out of phase with the grid voltage and then in phase after the additional load turns on. There is significant distortion in the current and voltage in the laboratory setup, due to large low frequency harmonics present in the utility power. The data presented in this paper has been filtered at 200 Hz to capture only the fundamental and lower frequency aspects of the current, voltage and power waveforms. Although distortion exists in the laboratory power source the experimental measurements shown in Figure 13 through Figure 15 demonstrate that the primary controller works as expected.

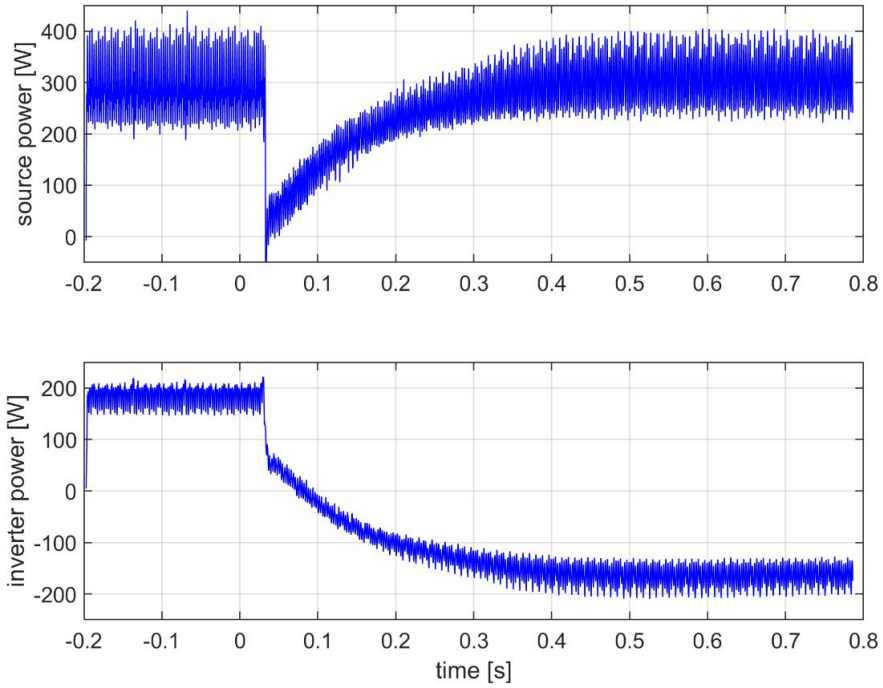

Figure 13. Source and inverter power when the additional load is disconnected.

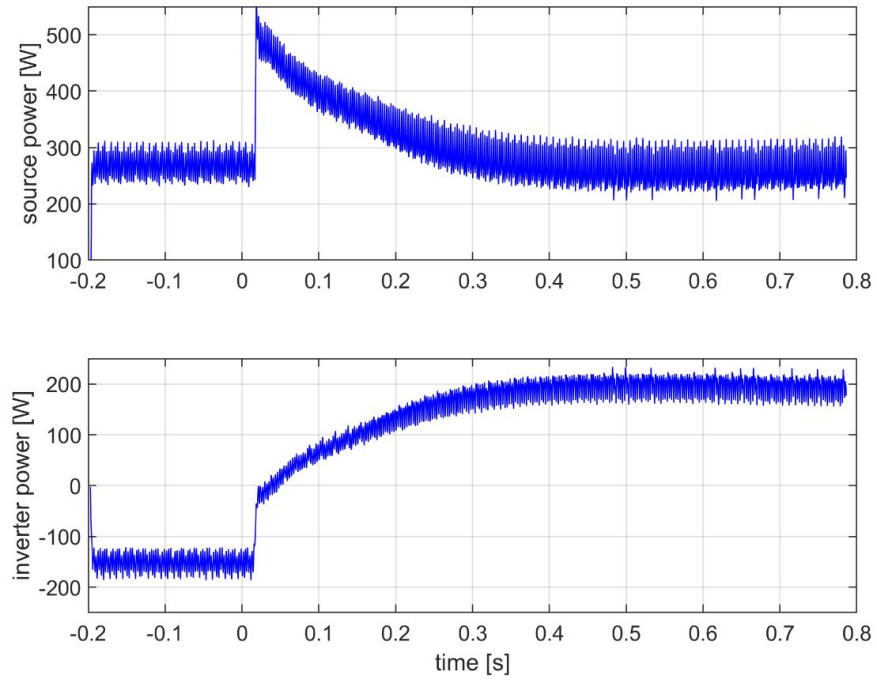

Figure 14. Source and inverter power when the additional load is connected.

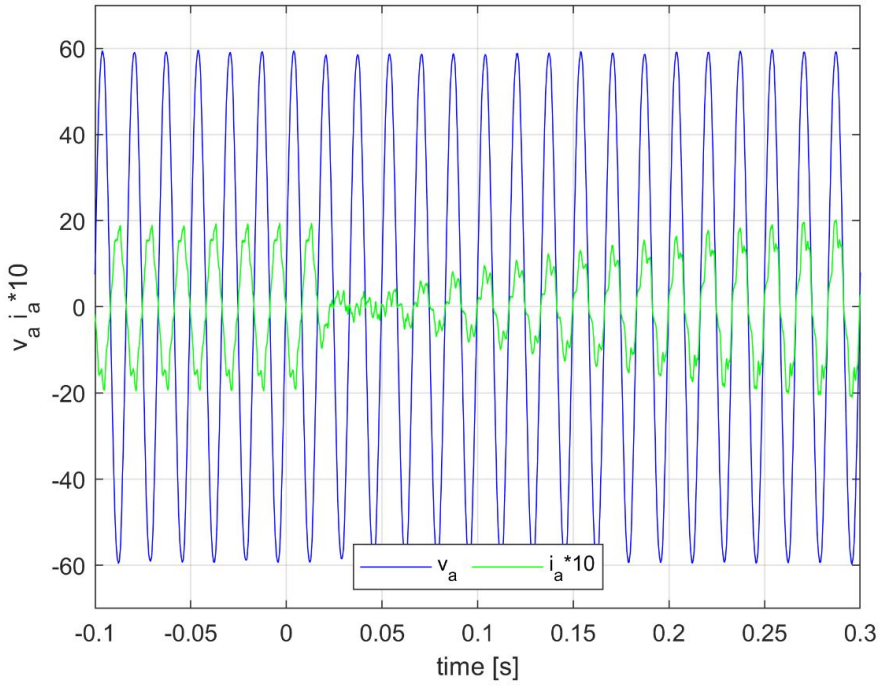

Figure 15. Inverter current (i_a) and grid voltage (v_a) when the additional load is connected.

6. A Few Economic Considerations, Supporting the Battery Sizing

From what results in Section 3.1, it is evident that the battery rated capacity is the smallest, when $\delta \approx \beta$, nevertheless the capacity is quite substantial and it takes as principal reference the daily GT production. In this work we want to support the new tailored EMS, by considering the role that storage can play, and viceversa. We do not aim at optimizing the sizing of each element, because we are retrofitting an existing layout, nevertheless we can support the choice which has been already done, by proposing a transition towards a microgrid, which is properly designed in those elements, which are the focus of this work. This transition is represented by the method to size the storage in combination with the EMS and this is the reason of mainly focusing on that. Hence, an intrinsic trade-off exists between its capital cost (depending on Q, capacity) and its estimated lifetime (depending on the DoD during cycling: the bigger Q, the smaller the experienced DoDs, thus the greater the expected lifetime). Additionally, the greater Q, the greater the saved curtailment and its economic value over the time horizon (T) the rig is operative. We have to notice that *over sizing* a battery is not the best definition of optimization, when the whole system can be optimized. But we, on the contrary, need to take action in a *situation* where only a new EMS and a new capacity for the storage can be proposed and justified. As a consequence, from the resulting over-sizing, or as we prefer to name it, *right*-sizing the storage, the system will operate by relying less on the full capacity of the battery. This will likely produce less deep discharges, which means more available cycling, thus extending its operating life and decreasing the rate of replacement over time. Of course also the WT production will be better exploited and stored, thus affecting the potential curtailment. Under these conditions, an effective step to evaluate this balance is to assess the net present value (NPV) of the extra investments on the batteries (which are often already included in the original configuration of the microgrid, for safety reasons), over the savings due to avoiding the WT curtailment and dissipative loads ($Savings_i$). The extra investment is due to the potential extra size of the storage, to the service of the WT, that otherwise could have been wasted on a dump load.

If the NPV is greater than zero over T (i = 1, . . .N), then the investment on a bigger storage (Inv^*_{bat} which depend on the size, thus Q) and eventually its replacement over the years of operation of the O&G rig (then r, discount rate is applied over the j years when the

replacement should occur for reaching the end-of-life of the battery due to its cycling), are worth the extra investment cost.

$$NPV(r, Q, T) = \sum_{i}^{N} Saving_i(r, Q) - Inv_{bat}^{0}(Q) - \sum_{j}^{J} Inv_{bat}^{j}(r, Q) \quad (24)$$

where J depends on the lifetime of the battery (in years) which in turn depends on the DoD. Specifically, I_{bat}^{0} is the investment on the storage at year 0, while I_{bat}^{j} are the storage replacement investments at the year j. The variable j depends on the DoD, thus on the cycling and the replacement intervals will be longer, if DoD are less deep. This is a way to procrastinate investments over time T. In fact, the bigger Q, the smaller the referenced DoD, thus the longer the alleged lifetime L_f.

$$roundup(T/L_f) = J \quad (25)$$

Literature reports hundreds of cases where the application of software like Homer, Retscreen, Hybrid 2, and Pvsyst, for example, is proposed and compared as well as literature where new proposals are born to support the economics of brand new hybrid configurations. A recent paper, [25] reviews many papers aiming at different targets, but none of them actually show the link we propose with this step-by-step analysis of a retrofitting microgrid. For instance, in [26] an optimal sizing of a multi-source power system including two different dynamics in term of storage energy is newly proposed -against the use of the software mentioned above- and a multi-objective based optimization algorithm is applied. Nevertheless the link between how to link primary and secondary control laws is missing and again the context differs from our focus on retrofitting with specific requirements.

7. Conclusions

This paper presents a solution which uses renewable energy sources to retrofit a microgrid installed on an offshore O&G rig. The proposed solution uses the maximum output of the renewable energy sources and leverages the following available tools: the integration of a "rightsizing" of the storage which guarantees no curtailment and no use of a dump load with the customized Energy Management System. We thus formulate an EMS which is identified by the methodology of rightsizing the integrated battery and also present a methodological approach to verify its economic use of fuel over the remaining time of operation T (depending -for instance- on the complete depletion of the field) of the O&G platform.

The novel contribution of the paper includes an experimentally-validated primary control system which minimizes fuel consumption and a customized EMS, which together eliminate the need for a dump load. Additionally, a battery sizing procedure is used in the economic system-level analysis to show the rational behind of the sizing choice. A selective choice of the components of the NPV formulation, focusing on the balancing between causes and effects in the costs and expected savings due to the storage integration is proposed to support the battery-sizing procedure, which unquestionably favors a surplus in capacity. Although a numerical example of the assessment is not reported here, because we sought to favour a methodological explanation, the well-known formulation is a valid tool to overcome the drawback/objection that our battery rightsizing may cause.

The proposed rightsizing of the battery allows it to operate with smaller DoD cycles, thus extending the lifetime of the batteries. Furthermore, by using more renewable energy production we inherently reduce fuel consumption and CO_2 emissions, making a step toward decarbonization of the service.

Author Contributions: Conceptualization, N.A. and G.O.; methodology, N.A.; software, N.A., S.R.D.S. and A.L.J.; validation, G.O. and A.L.J.; formal analysis, N.A. and S.R.D.S.; investigation, N.A., S.R.D.S., G.O. and A.L.J.; resources, N.A. and G.O.; data curation, N.A., S.R.D.S., G.O. and A.L.J.; writing—original draft preparation, N.A., S.R.D.S., G.O. and A.L.J.; writing—review and editing,

N.A., S.R.D.S., G.O. and A.L.J.; visualization, N.A., S.R.D.S. and G.O.; supervision, N.A. All authors have read and agreed to the published version of the manuscript.

Funding: This research received no external funding.

Data Availability Statement: Source data and code are available upon request from the authors.

Conflicts of Interest: The authors declare no conflict of interest.

Abbreviations

The following abbreviations are used in this manuscript:

BES	Battery Energy Storage System
DoD	Depth of Discharge
EMS	Energy Management System
GT	Gas Turbine
NPV	Net Present Value
O&G	Oil and Gas
PCC	Point of Common Coupling
PLL	Phase Locked Loop
SOC	State Of Charge
WT	Wind Turbine

References

1. Olivares, D.E.; Mehrizi-Sani, A.; Etemadi, A.H.; Cañizares, C.A.; Iravani, R.; Kazerani, M.; Hajimiragha, A.H.; Gomis-Bellmunt, O.; Saeedifard, M.; Palma-Behnke, R.; et al. Trends in Microgrid Control. *IEEE Trans. Smart Grid* **2014**, *5*, 1905–1919. [CrossRef]
2. Rocabert, J.; Luna, A.; Blaabjerg, F.; Rodríguez, P. Control of Power Converters in AC Microgrids. *IEEE Trans. Power Electron.* **2012**, *27*, 4734–4749. [CrossRef]
3. Parhizi, S.; Lotfi, H.; Khodaei, A.; Bahramirad, S. State of the Art in Research on Microgrids: A Review. *IEEE Access* **2015**, *3*, 890–925. [CrossRef]
4. Alam, M.S.; Arefifar, S.A. Energy Management in Power Distribution Systems: Review, Classification, Limitations and Challenges. *IEEE Access* **2019**, *7*, 92979–93001. [CrossRef]
5. Cheng, Z.; Duan, J.; Chow, M. To Centralize or to Distribute: That Is the Question: A Comparison of Advanced Microgrid Management Systems. *IEEE Ind. Electron. Mag.* **2018**, *12*, 6–24. [CrossRef]
6. de Matos, J.G.; e Silva, F.S.F.; d. S. Ribeiro, L.A. Power Control in AC Isolated Microgrids with Renewable Energy Sources and Energy Storage Systems. *IEEE Trans. Ind. Electron.* **2015**, *62*, 3490–3498. [CrossRef]
7. Solanki, B.V.; Bhattacharya, K.; Cañizares, C.A. A Sustainable Energy Management System for Isolated Microgrids. *IEEE Trans. Sustain. Energy* **2017**, *8*, 1507–1517. [CrossRef]
8. Arriaga, M.; Cañizares, C.A.; Kazerani, M. Northern Lights: Access to Electricity in Canada's Northern and Remote Communities. *IEEE Power Energy Mag.* **2014**, *12*, 50–59. [CrossRef]
9. The Microgrid Deployment Tracker 3Q22 by Guidehouse Insights. 2022. Available online: https://guidehouseinsights.com/reports/microgrid-deployment-tracker-3q22 (accessed on 10 October 2022).
10. Fard, R.N.; Tedeschi, E. Integration of distributed energy resources into offshore and subsea grids. *CPSS Trans. Power Electron. Appl.* **2018**, *3*, 36–45. [CrossRef]
11. Hu, D.; Zhao, X.; Xu, C.; Wang, J. Impact of wind power on stability of offshore platform power systems. In Proceedings of the 2008 Third International Conference on Electric Utility Deregulation and Restructuring and Power Technologies, Nanjing, China, 6–9 April 2008; pp. 1688–1692. [CrossRef]
12. He, W.; Jacobsen, G.; Anderson, T.; Olsen, F.; Hanson, T.D.; Korpås, M.; Toftevaag, T.; Eek, J.; Uhlen, K.; Johansson, E. The Potential of Integrating Wind Power with Offshore Oil and Gas Platforms. *Wind Eng.* **2010**, *34*, 125–137. [CrossRef]
13. Korpås, M.; Warland, L.; He, W.; Tande, J.O.G. A Case-Study on Offshore Wind Power Supply to Oil and Gas Rigs. *Energy Procedia* **2012**, *24*, 18–26. [CrossRef]
14. D'Arco, S.; Petterteig, A.; Pittini, R.; Undeland, T.M. Droop regulated VSCs for island operation of future offshore systems. In Proceedings of the 2011 IEEE Trondheim PowerTech, Trondheim, Norway, 19–23 June 2011; pp. 1–6. [CrossRef]
15. Årdal, A.R.; Undeland, T.; Sharifabadi, K. Voltage and Frequency Control in Offshore Wind Turbines Connected to Isolated Oil Platform Power Systems. *Energy Procedia* **2012**, *24*, 229–236. [CrossRef]
16. Silva, J.; Jafar, M.; Marichalar, A.; Tedeschi, E. Integration of Wind Power to Supply Water Injection Systems as Controllable Loads in Offshore Oil and Gas Facilities. In Proceedings of the Offshore Energy & Storage Symposium (OSES), Kalkara, Malta, 13–15 July 2016; pp. 1–9.
17. Sanchez, S.; Tedeschi, E.; Silva, J.; Jafar, M.; de Marichalar, A. Smart load management of water injection systems in offshore oil and gas platforms integrating wind power. *IET Renew. Power Gener.* **2017**, *11*, 1153–1162. [CrossRef]

18. Alves, E.; Sanchez, S.; Brandao, D.; Tedeschi, E. Smart Load Management with Energy Storage for Power Quality Enhancement in Wind-Powered Oil and Gas Applications. *Energies* **2019**, *12*, 2985. [CrossRef]
19. Anglani, N.; Di Salvo, S.R.; Oriti, G.; Julian, A.L. Renewable Energy Sources and Storage Integration in Offshore Microgrids. In Proceedings of the 2020 IEEE International Conference on Environment and Electrical Engineering and 2020 IEEE Industrial and Commercial Power Systems Europe (EEEIC/I CPS Europe), Madrid, Spain, 9–12 June 2020; pp. 1–6. [CrossRef]
20. Erickson, R.W.; Maksimovic, D. *Fundamentals of Power Electronics*; Springer Science & Business Media, LLC: New York, NY, USA, 2001.
21. O'Rourke, C.J.; Qasim, M.M.; Overlin, M.R.; Kirtley, J.L. A Geometric Interpretation of Reference Frames and Transformations: dq0, Clarke, and Park. *IEEE Trans. Energy Convers.* **2019**, *34*, 2070–2083. [CrossRef]
22. Epoupa Mengou, J.; Gambaro, C.; Alessi, A.; Terenzi, A.; Vecchione, M.; Binaschi, M.; Di Salvo, S.R.; Anglani, N. A Case-Study for the Reduction of CO_2 Emissions in an Offshore Platform by the Exploitation of Renewable Energy Sources Through Innovative Technologies Coupled with Energy Storage. In Proceedings of the Abu Dhabi International Petroleum Exhibition and Conference, Abu Dhabi, United Arab Emirates, 18 November 2021.
23. Binaschi, M. Integrazione di una boa Wave Energy Converter in una Microrete Isolata: Analisi di Metodologie per il Calcolo della Potenza Erogata in Funzione delle Condizioni del Mare. Master's Thesis, University of Pavia, Pavia, Italy, 2020.
24. Anglani, N.; Oriti, G.; Colombini, M. Optimized energy management system to reduce fuel consumption in remote military microgrids. In Proceedings of the 2016 IEEE Energy Conversion Congress and Exposition (ECCE), Milwaukee, WI, USA, 18–22 September 2016; pp. 1–8. [CrossRef]
25. Khan, A.A.; Minai, A.F.; Pachauri, R.K.; Malik, H. Optimal Sizing, Control, and Management Strategies for Hybrid Renewable Energy Systems: A Comprehensive Review. *Energies* **2022**, *15*, 6249. [CrossRef]
26. Abdelkader, A.; Rabeh, A.; Mohamed Ali, D.; Mohamed, J. Multi-objective genetic algorithm based sizing optimization of a stand-alone wind/PV power supply system with enhanced battery/supercapacitor hybrid energy storage. *Energy* **2018**, *163*, 351–363. [CrossRef]